# Onset of vortex clustering and inverse energy cascade in dissipative quantum fluids

R. Panico,[1,2] P. Comaron,[3,4] M. Matuszewski,[3] A. S. Lanotte,[1,5] D. Trypogeorgos,[1]
G. Gigli,[1,2] M. De Giorgi,[1] V. Ardizzone,[1,2] D. Sanvitto,[1,*] and D. Ballarini[1,†]

[1]*CNR NANOTEC, Institute of Nanotechnology, Via Monteroni, 73100 Lecce, Italy*

[2]*Dipartimento di Matematica e Fisica E. De Giorgi, Università del Salento,*
*Campus Ecotekne, via Monteroni, Lecce 73100, Italy*

[3]*Institute of Physics, Polish Academy of Sciences,*
*Al. Lotników 32/46, 02-668 Warsaw, Poland*

[4]*Department of Physics and Astronomy,*
*University College London, Gower Street,*
*London, WC1E 6BT, United Kingdom*

[5]*INFN, Sez. Lecce, 73100 Lecce, Italy*

## Abstract

Turbulent phenomena are among the most striking effects that both classical and quantum fluids can exhibit. While classical turbulence is ubiquitous in nature, the observation of quantum turbulence requires the precise manipulation of quantum fluids such as superfluid helium or atomic Bose-Einstein condensates. In this work we demonstrate the turbulent dynamics of a 2D quantum fluid of exciton-polaritons, hybrid light-matter quasiparticles, both by measuring the kinetic energy spectrum and showing the onset of vortex clustering. We demonstrate that the formation of clusters of quantum vortices is triggered by the increase of the incompressible kinetic energy per vortex, showing the tendency of the vortex-gas towards highly excited configurations despite the dissipative nature of our system. These results lay the basis for the investigations of quantum turbulence in two-dimensional fluids of light.

The complex dynamics of turbulent flow has repeatedly attracted the interest of scientists across many fields of research [1]. The experimental investigation of quantum fluid dynamics started with the evidence of quantised vortices in superfluid helium [2, 3], following the theoretical speculations of Feynman [4]. Despite important differences, quantum turbulence shares observables with its classical counterpart and allows a simpler description in terms of vortices with unitary topological charge [5, 6]. Since the observation of Bose-Einstein condensates (BECs) of ultracold atoms [7, 8], BECs have become a well-established platform for the study of quantum turbulence [9, 10]. Recently, the ability to form highly oblate BECs boosted the research on vortex clustering [11–16], an elusive feature of two-dimensional quantum turbulence (2DQT) strongly related to the inverse energy cascade observed in classical 2D turbulence [17]. The inverse energy cascade, as opposed to the direct cascade, involves the energy transfer from small to larger scales and manifests in the universal Kolmogorov-like $-5/3$ power law scaling of the kinetic energy spectrum [18]. Onsager proposed an explanation for this counter-intuitive phenomenon by applying equilibrium statistical mechanics to a model of point-like vortices: in a closed and conservative system, the formation of vortex clusters is the result of a transition to a thermal equilibrium state which comprises more energy but less entropy (resulting in a negative absolute temperature) as compared to a configuration of randomly distributed vortices [19]. Quantum vortex clustering and negative temperature regimes were realized only recently in atomic BECs thanks to finely-tuned excitation conditions [20, 21]. However, the direct measurement of the kinetic energy

spectrum and the inverse cascade in 2DQT is still challenging. Optical systems, such as quantum fluids of light, are intriguing alternatives in this direction, since it is possible to directly measure the phase of the quantum fluid and its velocity field [22–26].

As a paradigmatic family of quantum fluids of light, here we study exciton-polaritons— bosonic quasi-particles which result from the strong interaction between light and matter in semiconductor microcavities with embedded quantum wells [27]. The formation of solitons and vortices in polariton superfluids has been observed under different configurations, including spontaneous formation due to local density flows, nucleation in the wake of an obstacle and direct imprinting via phase mapping [28–31]. Notably, polaritons are strictly 2D, being confined in the plane of the cavity, and the potential landscape can be designed at will by both all-optical and lithographic techniques, potentially enabling strong connections between topological photonics and 2DQT [32–34]. Few works, however, have addressed polariton superfluids in the general context of turbulent dynamics. This is because polariton superfluids, unlike atomic BECs, are inherently dissipative, with the polariton lifetime limited in the picoseconds time range by the photon leakage from the microcavity or the non-radiative exciton decay. This raises the question whether 2DQT is even observable in this regime and, in the affirmative case, what are the main differences as compared to a conservative system [35–37]. Theoretically, the turbulent dynamics of out-of-equilibrium condensates were first studied by Berloff [38] and, more recently, Koniakhin *et al.* simulated the 2DQT energy spectrum of polariton superfluids in the conservative limit of long polariton lifetime [39]. Despite both these works suggesting that turbulent regimes are indeed possible in polariton fluids, no experimental evidence has been reported so far.

In this work we show both the onset of vortex clustering and inverse energy cascade in a polariton quantum fluid. To overcome the intrinsic time limit imposed by dissipation, we create a highly energetic initial state by injecting a polariton superfluid against a potential barrier. Indeed, two dynamical processes compete: the build-up of energy at larger spatial scales, and the polariton dissipation which weakens the growth of spatial correlations among vortices. We demonstrate that the initial kinetic energy provided to the superfluid is crucial to form a dense vortex gas and accelerate the formation of clusters. These observations are confirmed using numerical simulations of the polariton nonlinear Schroedinger equation.

*System.* - In quantum fluids, the formation of clusters of same sign vortices is often seen as the statistical signature of the inverse energy cascade. Indeed, clustering not only limits
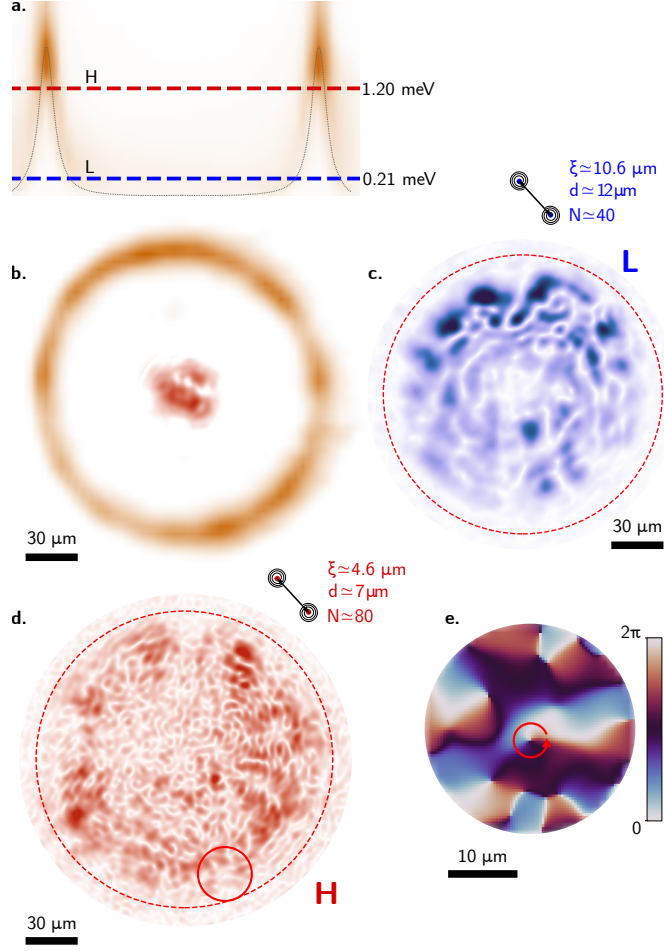
FIG. 1. **Fig. 1: Injection and trapping of a polariton quantum fluid. a.** Energy resolved photoluminescence of a vertical slice of the ring-shaped potential barrier, created upon non-resonant excitation of the sample. The blue and red dashed lines indicate the injection energies of the superfluid labeled as L and H respectively. **b.** Superposition of the image of the trap in real space and the measured density of the polariton superfluid taken 2 ps after the injection with a pulsed laser. **c., d.** Time frame of the polariton density taken at 60 ps after the injection for the low (c) and high (d) detuning; $N$ denotes the total number of vortices, $d$ the mean distance between nearest neighbouring vortices and $\xi$ the healing length. The red dashed circle represents the position of the potential barrier. **e.** Phase of the superfluid corresponding to the red solid circle in (d). Vortices can be identified by a $2\pi$ change of the circulation.

pair-vortex annihilations and the consequent phonon emission, but drives the system to a highly energetic state [40, 41]. To check if similar dynamics can be observed in a dissipative quantum fluid, the system needs to be initialized in a highly excited state. To this aim, we inject polaritons in a high Q-factor ($> 10^5$) microcavity [42] by using a 2 ps pulsed laser beam focused at the center of a ring-shaped potential barrier as shown in Fig. 1a-b (further details can be found in the Methods section). The detuning of the pulsed beam from the bottom of the potential barrier corresponds to the initial kinetic energy of the polariton fluid, which expands radially after the injection, until it reaches the ring barrier [43, 44] (additional details in Note S1 and Fig. S1 of the Supplementary Information). To assess the role of the initial energy on the dynamics of the vortex gas, we consider two injection energies $\delta E$ from the bottom of the potential, namely $\delta E_L = 0.21$ meV and $\delta E_H = 1.2$ meV, henceforth referred to as L and H, which are indicated in Fig. 1a by the blue and the red horizontal dashed lines, respectively. The temporal evolution of the vortex gas after the collision with the potential barrier is followed using off-axis digital holography [45]. This interferometric technique allows us to obtain a time resolution comparable to the pulse length and enables the direct measurement of both the polariton density and the polariton phase distributions at each time frame with sub-healing length spatial resolution (additional details in Note S2 and Fig. S2 of the Supplementary Information). The vortex dynamics are initiated after an initial expansion time of approximately 40 ps for the H case and 50 ps for the slower-expanding fluid in the L case.

A snapshot of the 2D polariton density after 60 ps from the injection is shown for the L and H configurations in Fig. 1c and Fig. 1d, respectively. The identification of the vortex positions, including their circulation direction, is realized by searching for an exact $2\pi$ circulation of the phase around each point (Fig. 1e). Since the net angular momentum of our experiment is zero, the system nucleates only vortex-antivortex pairs (dipoles), preserving the neutrality of the charge throughout the whole dynamics. In the following, we analyse the spatial configuration of the vortex gas and compare its temporal evolution for L and H initial conditions.

*Vortex classification and energy decomposition.* - To study the ordering of our system we classify the phase singularities into three different categories: free vortices, dipole pairs, and clusters of the same sign [12, 20, 46]. Figure. 2a shows a typical result of this analysis applied to a time frame corresponding to 70 ps after the pulsed excitation. The vortex

positions are indicated by dots, while the streamlines in the background are the velocity field $\mathbf{v}(\mathbf{r}, t) = \frac{\hbar}{m} \nabla \phi(\mathbf{r}, t)$, with $m$ the polariton mass, as directly obtained from the measured phase $\phi(\mathbf{r}, t)$ of the polariton fluid. In H, the total number of vortices formed after the collision with the border of the ring is larger ($\approx 80$) than L ($\approx 40$) due to the higher expansion velocity of the fluid. As can be seen from the color code in Fig. 2a, vortices mostly belong to dipoles in the upper panel (L), as opposed to the lower panel (H) where the number of vortices in clusters, dipoles and free vortices is comparable.

Before discussing the temporal evolution, let us stress the importance of being able to easily measure the phase of the superfluid $\phi(\mathbf{r}, t)$ at any time interval. This allows us to separate the contribution to the total kinetic energy due to the presence of quantum vortices from that coming from the sound waves [47]. Indeed, applying the Helmholtz decomposition one can separate the divergence-free (incompressible) and the irrotational (compressible) part of the superfluid velocity associated with the vortex distribution and the sound waves, respectively (see Note S3 and Note S4 of the Supplementary Information). In the next section, we use the incompressible velocity field to compare the information on the kinetic energy with the vortex classification analysis. In Fig. 2b, the result of the velocity decomposition as extracted from the experimental data are shown for a portion of the fluid in H (dashed circle). The bright points in the bottom panel of Fig. 2b correspond to singularities in the polariton phase. In the tracking and classification analysis, we consider only those vortices with cores separated by a distance larger than the healing length, $\xi = \hbar/(2mg|\psi|^2)^{1/2}$, with $g$ the interaction constant and $|\psi|^2$ the density of polaritons (see Methods).

*Temporal evolution and onset of clustering.* -   The vortex tracking allows us to compute the correlation function $C = \frac{1}{N} \sum_{i=1}^{N} c_i$ for each time frame, with $N$ the total vortex number and $c_i = 1$ if the circulation of the nearest neighbor of the i-th vortex has the same sign, or $c_i = -1$ if it has the opposite sign. Increasing values of C correspond to higher energetic states of the vortex gas. In the Onsager model, negative temperatures are associated to $C > 0$, whereas $C = 0$ corresponds to the infinite temperature limit (maximum entropy) and $C = -1$ is the lowest (positive) temperature [14, 15, 18]. Typically, during the spontaneous evolution of a polariton fluid, $C$ is negative and tends towards the lowest energy state, $C = -1$, due to the dissipative nature of the system and the spontaneous nucleation of dipoles (see Note S5 and Fig. S3 of the Supplementary Information). In Fig. 2c, we show instead that $C$ reaches values close to $C = 0$ between 40 ps and 80 ps (red points), suggesting that,
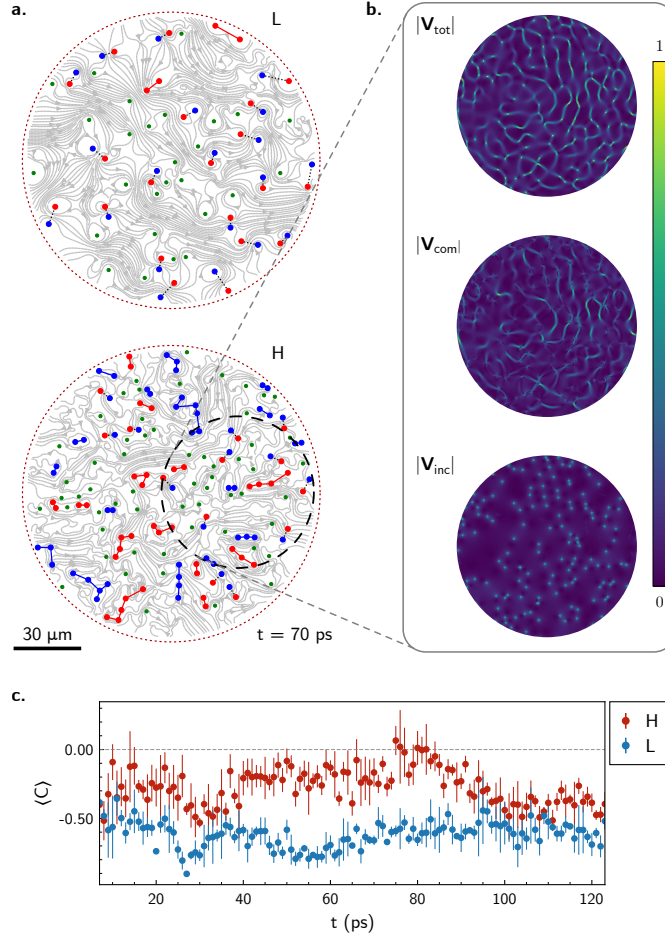
FIG. 2. **Fig. 2: Vortex classification and velocity decomposition. a.** Distribution of vortices at low (L, top panel) and high (H, bottom panel) injection energies taken at t = 70 ps after the injection time. Blue and red dots represent positive and negative winding vortices belonging to dipoles (black dashed lines) or clusters (solid lines) respectively. For free vortices (green dots), the sign is not reported. The streamlines in the background show the incompressible velocity field of the superfluid. **b.** Velocity field decomposition of a portion of the superfluid in panel (a). The three figures show the modulus of the total velocity (top panel), in addition to the compressible (middle) and incompressible (bottom) components. The modulus of the velocity is normalised for each panel. **c.** Vortex first order correlation functions for high and low injection energy shown as the mean over different realizations ($n = 4$) by red and blue points, respectively, with their standard deviations (SD).
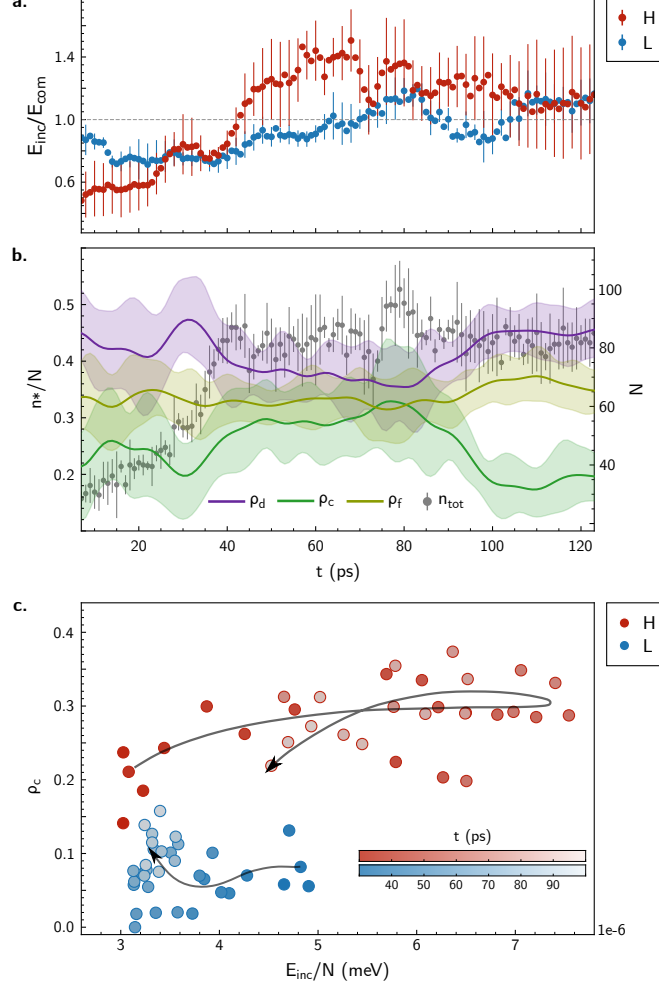
FIG. 3. **Fig. 3: Energy transfer and clusterization. a.** Ratio between the mean values of the incompressible and compressible kinetic energy for the two configurations shown as points ± SD ($n = 4$). For the sake of clarity, we provided the error bars at each alternate point; the missing ones are comparable to those displayed. **b.** Mean values of the fractions of dipoles ($\rho_d$, purple line), clusters ($\rho_c$, green line) and free vortices ($\rho_f$, yellow line) for the H configuration. The temporal resolution is the same as in every other figure and the respective standard deviations are represented by shadowed regions. The mean total number of vortices in time is shown by the scatter gray dots with their respective SD. The sample size is the same as in (a) **c.** Relative number of clusters versus mean incompressible energy per vortex in both the L and H case. Arrows represent the direction of time.

despite the finite polariton lifetime ($\approx 100\,\mathrm{ps}$), the vortex gas evolves towards more energetic configurations. In the dynamical evolution, clustering competes with other processes, the main one being the polariton losses which causes the growth of the healing length and makes the inverse cascade even more energetically expensive. In the presence of losses, the correlation C initially increases towards higher values and remains approximately constant for a transient time, as shown in Fig. 2c. After 80 ps, eventually dissipation prevails and correlations start decreasing. This behavior is visible only in H (red points in Fig. 2c), while in L (blue points) the correlation function is $C \approx -0.7$ throughout the dynamics.

The increase of $C$ requires the injection of incompressible kinetic energy into the system. In a closed system such as an atomic BECs, even in the absence of a constant energy injection, this is explained by means of an evaporative-heating mechanism [14]. The vortex gas undergoes vortex-pair annihilation while conserving the total energy of the system, leading to an increase of the mean energy per vortex. Therefore, the number of vortices decreases with time, and the few remaining vortices tend to form small clusters [20, 48]. In our open system, the simultaneous presence of sound waves and vortices leads to additional mechanisms of energy transfer. In fact, the interplay between the different contributions to the total energy in compressible quantum fluids is crucial to the study of turbulent dynamics and it has only recently been addressed theoretically [49]. In the following, we show that the kinetic energy of sound waves is efficiently transformed into kinetic energy of the vortex gas.

In Fig. 3a, the ratio of the compressible and incompressible kinetic energy is shown for H and L as a function of time. In H (red points), the compressible component is transformed into incompressible kinetic energy, which becomes dominant starting from 40 ps. On the contrary, in L (blue points), the sound waves component is higher than the incompressible one during the whole dynamics, becoming roughly the same at later times. In Fig. 3b, the three vortex species fractions, namely dipoles ($\rho_d$), clusters ($\rho_c$), and free vortices ($\rho_f$) are shown for the H configuration, along with the total number of vortices (dotted line). While in the first 40 ps the increase of the incompressible kinetic energy occurs through the nucleation of new vortices, the further increase up to 80 ps occurs with a constant number of total vortices. In this time-interval, the increase of the number of clusters occurs at the expense of dipoles, showing that the additional incompressible kinetic energy forces the vortex gas to form small clusters, as opposed to L configuration (see Note 6 and Fig. S4

9

of the Supplementary Information). This behaviour is displayed in Fig. 3c, where we plot the clustered fraction of vortices versus the average incompressible kinetic energy *per vortex*, showing the opposite dynamical evolution of H and L configurations.

*Energy spectrum.* - Figure 4a shows the incompressible kinetic energy spectrum measured in H and L configurations between 60 ps and 80 ps. The appearance of a Kolmogorov-like $k^{-5/3}$ scaling law (horizontal, dashed-black line), associated with the inverse energy cascade [18, 50], is clearly visible in H at wavevectors smaller than $k_\xi$, the inverse of the healing length. It is noteworthy that in spite of the small range of scale involved, this is the first direct measurement of an energy spectrum showing the inverse cascade in a 2D quantum fluid.

In the ultraviolet range $k > k_\xi$, both H and L show a $k^{-3}$ decay (dotted black line), the expected scaling law associated to the internal structure of a quantum vortex [11]. Different behaviour are instead observed for wavevectors smaller than $k_\xi$. In L, the infrared spectrum ($k < k_\xi$) tends towards $k^{-1}$ (solid black line), which can be derived from the velocity distribution of a collection of vortices in the far-field [11]. On the contrary, in H, we observe the $k^{-5/3}$ scaling extending from $k_c < k < k_\xi$, with $k_c$ approximately corresponding to the inverse of the typical spatial size of the clusters, $l_c \simeq$ (3-4)$\xi$. In Fig. 4b, to highlight the microscopic mechanism of energy transfer to larger scales, we show the incompressible velocity field, as extracted directly from the experiment in H, around a dipole and a cluster of three vortices. In the dipole, the two vortices are closer to each other and the maximum of the velocity is observed between them; whereas in the cluster, the velocity field is arranged on a larger spatial scale, with the flow circulating externally to the three vortices. Dimensional analysis shows that the time required to form clusters of that size is of about 20 ps in our system (see Note S7 of the Supplementary Information), which is comparable with the measured time interval after the expansion in our measurements. In Fig. 4c, by integrating over different time intervals, we show how the Kolmogorov-like scaling law emerges over time as the energy is gradually transferred to larger scales.

Finally, we note that the energy spectrum is taken directly from spatial differentiation of the measured phase, without any knowledge about the number and relative distances between vortices. The independent observation of vortex clustering and inverse cascade spectrum provides a direct link between the two descriptions of 2DQT, the one related to Onsager point-vortex model and that of the inverse cascade of incompressible kinetic energy.
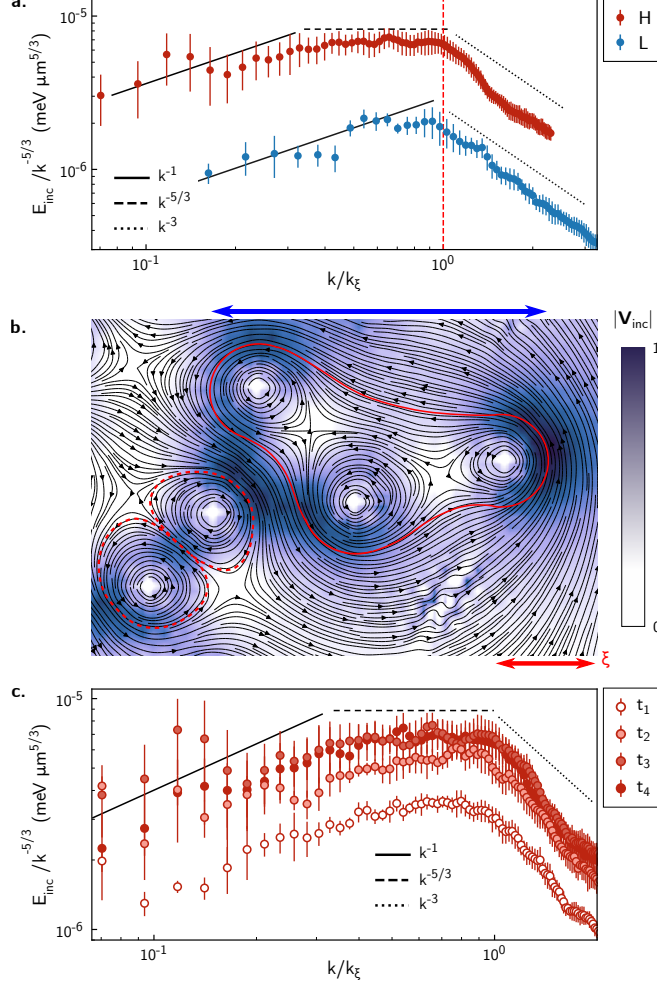
FIG. 4. **Fig. 4: Inverse energy cascade. a.** Energy spectrum for H (red) and L (blue), integrated in the time interval between 60 ps and 80 ps, reported as a mean $(n = 4) \pm$ SD. The $k$-axis is rescaled to account for the different healing length (represented by a red dashed line) in H and L (see Methods). The black and gray straight lines, which represent the power scaling laws, are just meant as guidelines. **b.** The incompressible velocity field around a configuration made of a dipole (dashed red line) and a cluster of three vortices with the same sign (solid red line). The background heat map represents the modulus of the incompressible velocity. To enhance the visibility, the region close to the vortex core is filtered out and the map is saturated at $|V_{inc}| = 1.6 \, \mu m \, ps^{-1}$. The "size" of the cluster, indicated by the blue line, is $\sim 3.4 \, \xi$. **c.** Time evolution of the energy spectrum for H that shows the buildup of the inverse energy cascade. The time intervals shown are $t_1 = 34$–44 ps, $t_2 = 47$–57 ps, $t_3 = 60$–70 ps and $t_4 = 70$–80 ps. Error bars are defined as in (a). All spectra are normalised by the number of particles, as discussed in the Methods section.

11

To confirm our findings, we perform simulations of the Gross-Pitaevskii equation for the polariton field [51]. The appearance of the $k^{-5/3}$ scaling law in the incompressible kinetic energy spectrum is observed in numerical simulations and corresponds to an increase of both the correlation function and the incompressible kinetic energy per vortex (Fig. S6 of the Supplementary Information). As observed in both experiments and simulations, the dynamics is faster when the polariton density is larger and the intervortex distance is comparable to the healing length, resulting in an effective increase of the interactions between vortices. Moreover, we check with simulations that a moderate sample inhomogeneity allows the detection of random vortices even after averaging over many independent realisations, as already anticipated in previous works [52, 53] (further details in the Methods and Note S9 of the Supplementary Information).

In conclusion, in this work we demonstrate the possibility of exploring turbulent states in quantum fluids of light. These results show the first evidence of the inverse energy cascade in dissipative quantum fluids, along with the onset of vortex clustering on timescales of few tens of picoseconds. Importantly, we can decouple the compressible and incompressible contributions to the kinetic energy, showing that the energy required to start the clusterization dynamics is provided to the vortex gas by the dissipation of sound waves. Finally, we show that the optical measurement of the velocity field allows an unprecedented control over the dynamics of the vortex gas, enabling a new series of experiments to be performed in nonlinear optical systems such as semiconductor microcavities, nonlinear crystals, and laser beams coupled to hot atomic vapours or Rydberg atomic states [54–57].

*Methods. -*

**Experiment:** The ring potential (diameter $R \simeq 150$ µm) is realized by shaping a continuous-wave (CW) laser beam ($\lambda = 735$ nm) with a spatial light modulator. The local energy shift of the polariton resonance, due to the high exciton density induced by the CW pump, is able to confine the polariton superfluid within the potential barrier (Fig. 1a). The polariton superfluid is quasi-resonantly injected ($\lambda \approx 773$ nm) by focusing a pulsed beam (pulse length $\sim 2$ ps) in a Gaussian spot with a beam radius $w \simeq 17$ µm at the center of the ring potential (Fig. 1b). Given the repetition rate of the pulsed pump (80 MHz) and the typical integration time of 1 ms, each time frame is obtained from the integration of a

large number of pulses, giving as a result the average vortex distribution averaged over a large number of events. This is required since a single realisation would not provide enough signal to be detected. The time-resolved 2D map of the polariton fluid is obtained by averaging, for each time frame, over many pulses directly on the CCD camera. The vortex can be detected despite the averaging over many realisations thanks to the unavoidable presence of spatial inhomogeneity, which allows the observation of coherent realisations of the spontaneous vortex dynamics [52] (see Note S9 of the Supplementary Information). Our analysis is the result of an average of four measurements for each case, obtained by translating the sample in plane to exclude effects due to its morphology. Moving onto a different location of the sample, we obtain different spatial configurations, whose statistical properties are however unchanged, confirming the statistical significance of the observables. The sample used is a planar $Al_x Ga_{1-x} As$ microcavity with aluminium fractions of 0.2 and 0.95 in the distributed Bragg reflectors and 12 quantum wells of GaAs embedded in the cavity layer. The sample is kept at a cryogenic temperature of $\sim 5$ K. The measurements are taken in reflection configuration, with counter-polarized detection with respect to the polarization of the exciting laser. This is possible due to the precession of the polarization typically observed in polariton microcavity as a consequence of TE-TM splitting [58].

From the separation of scales observed in the energy spectrum (Fig. 4a) we are able to estimate the healing length in the 60–80 ps interval to be $\xi \simeq 4.6$ µm in H and $\xi \simeq 10.6$ µm in L.

In the energy decomposition, the density of the system is normalised at each time frame so that $\int \rho(\mathbf{x}) d\mathbf{x} = 1$, to rule out non-relevant physical behaviours stemming from the modulation of the density throughout the evolution due to the measurement technique employed.

In Fig. 4a, the energy spectrum is displayed for a range of wavevectors that spans from the inverse diameter of the trap $k_t = 2\pi/R$ to $k_r = 2\pi/r$, with $r = 3$ µm (slightly more than the optical resolution of our optical setup $\sim 2$ µm), both rescaled by the respective $k_\xi = 2\pi/\xi$ for H and L.

**Simulations:** To further confirm our findings, we perform simulations of the equation of motions for the polariton field $\psi = \psi(\mathbf{r}, t)$ with the generalised polariton Gross-Pitaevski

equation [23, 51], which at a mean-field level reads ($\hbar = 1$):

$$id\psi_c = dt\left[-\frac{\nabla^2}{2m} + g|\psi_c|^2 + \frac{i}{2}\gamma_c + V(\mathbf{r})\right]\psi_c \qquad (1)$$

where $m$ is the polariton mass; $g$ is the polariton-polariton interaction strength; $\gamma_c = 1/\tau_c$ is the polariton loss rate, corresponding to the inverse of the polariton lifetime $\tau_c$. In the Supplementary Information (Note 8) we compare and discuss the results obtained with Eq. (1) with those achieved within the Truncated Wigner approximation, a beyond mean-field theoretical formulation which accounts for quantum fluctuations [23].

Parameters are chosen to correspond with the microcavity used in the experiments, and reads $m = 0.22$ ps meV $\mu$m$^{-2}$ = $3.5210^{-35}$ kg, $g = 5 \times 10^{-3}$ meV $\mu$m$^2$. The fluid of light is confined in a hard-bounded annular potential $V(\mathbf{r})$ with a radius $r = 70$ $\mu$m.

The dynamics is initiated by a central Gaussian profile, providing the initial expansion. Its local phase is constant throughout space thus accounting for the quasi-resonant nature of the initial experimental impulse. The increase of the detuning of the pump in the experimental case is controlled by the intensity of the initial profile, which also corresponds to an increment of the density of particles as well as the velocity of the outward particle flux. Simulations for different blue-shifts are found to be in good agreement with the experimental results as shown in Figs. 3, 4, and Figs. S5, S6 in the SI. In Fig. 3b-c and Fig. S6d-e (SI), the fraction of vortices belonging to clusters is shown in experiments and simulations, respectively. Increasing the injection energy, the formation of clusters is faster and occurs with higher probability. The faster dynamics is driven by stronger interactions between vortices, which are effectively increased at lower intervortex distances (i.e. when the total vortex density is increased), as observed in both experiments and simulations (Fig. 3b and Fig. S6a in SI). The relation between clusterization and vortex density is confirmed by additional analysis reported in the supplementary text.

*Data availability* -   The data that support the findings of this study are available from the authors upon reasonable request.

*Code availability* -   The codes used in this study will be provided upon reasonable request.

*Author contributions -* RP, PC, MM, DB, DS contributed to the formulation of the project. MM, DB, DS supervised the project. RP, PC contributed to the data curation and together with ASL, DB to the formal analysis and development of the methodology. RP, PC, DT cured the codes. Funding acquisition was managed by MM, DS, GG. All authors contributed to the discussions and the review of the manuscript.

*Competing interests -* Authors declare that they have no competing interests.

---

\* Corresponding author: daniele.sanvitto@cnr.it

† Corresponding author: dario.ballarini@nanotec.cnr.it

[1] U. Frisch, *Turbulence: The Legacy of A. N. Kolmogorov* (Cambridge University Press, 1995).

[2] H. E. Hall, W. F. Vinen, and D. Shoenberg, The rotation of liquid helium II II. The theory of mutual friction in uniformly rotating helium II, Proceedings of the Royal Society of London. Series A. Mathematical and Physical Sciences **238**, 215 (1956).

[3] C. F. Barenghi, L. Skrbek, and K. R. Sreenivasan, Introduction to quantum turbulence, Proceedings of the National Academy of Sciences **111**, 4647 (2014).

[4] R. P. Feynman, Application of quantum mechanics to liquid helium, in *Progress in Low Temperature Physics*, Vol. 1, edited by C. J. Gorter (Elsevier, 1995) Chap. 2, pp. 17–53.

[5] C. F. Barenghi and N. G. Parker, *A primer on Quantum Fluids* (Springer, 2016).

[6] M. Tsubota, Quantum turbulence, Journal of the Physical Society of Japan **77**, 111006 (2008).

[7] M. H. Anderson, J. R. Ensher, M. R. Matthews, C. E. Wieman, and E. A. Cornell, Observation of Bose-Einstein condensation in a dilute atomic vapor, Science **269**, 198 (1995).

[8] K. B. Davis, M. O. Mewes, M. R. Andrews, N. J. van Druten, D. S. Durfee, D. M. Kurn, and W. Ketterle, Bose-Einstein condensation in a gas of sodium atoms, Phys. Rev. Lett. **75**, 3969 (1995).

[9] E. A. L. Henn, J. A. Seman, G. Roati, K. M. F. Magalhães, and V. S. Bagnato, Emergence of turbulence in an oscillating Bose-Einstein condensate, Phys. Rev. Lett. **103**, 045301 (2009).

[10] A. C. White, B. P. Anderson, and V. S. Bagnato, Vortices and turbulence in trapped atomic condensates, Proceedings of the National Academy of Sciences **111**, 4719 (2014).

[11] A. S. Bradley and B. P. Anderson, Energy spectra of vortex distributions in two-dimensional quantum turbulence, Phys. Rev. X **2**, 041001 (2012).

[12] M. T. Reeves, T. P. Billam, B. P. Anderson, and A. S. Bradley, Inverse energy cascade in forced two-dimensional quantum turbulence, Phys. Rev. Lett. **110**, 104501 (2013).

[13] T. P. Billam, M. T. Reeves, B. P. Anderson, and A. S. Bradley, Onsager-Kraichnan condensation in decaying two-dimensional quantum turbulence, Phys. Rev. Lett. **112**, 145301 (2014).

[14] T. Simula, M. J. Davis, and K. Helmerson, Emergence of order from turbulence in an isolated planar superfluid, Phys. Rev. Lett. **113**, 165302 (2014).

[15] A. J. Groszek, M. J. Davis, D. M. Paganin, K. Helmerson, and T. P. Simula, Vortex thermometry for turbulent two-dimensional fluids, Phys. Rev. Lett. **120**, 034504 (2018).

[16] J. Han and M. Tsubota, Onsager vortex formation in two-component Bose–Einstein condensates, Journal of the Physical Society of Japan **87**, 063601 (2018).

[17] G. Boffetta and R. E. Ecke, Two-dimensional turbulence, Ann. Rev. Fluid Mech. **44**, 427 (2012).

[18] R. H. Kraichnan, Inertial ranges in two-dimensional turbulence, The Physics of Fluids **10**,

1417 (1967).

[19] L. Onsager, Statistical hydrodynamics, Il Nuovo Cimento **6**, 279 (1949).

[20] S. P. Johnstone, A. J. Groszek, P. T. Starkey, C. J. Billington, T. P. Simula, and K. Helmerson, Evolution of large-scale flow from turbulence in a two-dimensional superfluid, Science **364**, 1267 (2019).

[21] G. Gauthier, M. T. Reeves, X. Yu, A. S. Bradley, M. A. Baker, T. A. Bell, H. Rubinsztein-Dunlop, M. J. Davis, and T. W. Neely, Giant vortex clusters in a two-dimensional quantum fluid, Science **364**, 1264 (2019).

[22] F. T. Arecchi, G. Giacomelli, P. L. Ramazza, and S. Residori, Vortices and defect statistics in two-dimensional optical chaos, Phys. Rev. Lett. **67**, 3749 (1991).

[23] I. Carusotto and C. Ciuti, Quantum fluids of light, Rev. Mod. Phys. **85**, 299 (2013).

[24] Q. Fontaine, T. Bienaimé, S. Pigeon, E. Giacobino, A. Bramati, and Q. Glorieux, Observation of the Bogoliubov dispersion in a fluid of light, Phys. Rev. Lett. **121**, 183604 (2018).

[25] D. Ballarini, D. Caputo, G. Dagvadorj, R. Juggins, M. D. Giorgi, L. Dominici, K. West, L. N. Pfeiffer, G. Gigli, M. H. Szymańska, and D. Sanvitto, Directional Goldstone waves in polariton condensates close to equilibrium, Nature Communications **11**, 217 (2020).

[26] F. E. Öztürk, T. Lappe, G. Hellmann, J. Schmitt, J. Klaers, F. Vewinger, J. Kroha, and M. Weitz, Observation of a non-hermitian phase transition in an optical quantum gas, Science **372**, 88 (2021).

[27] A. Amo, D. Sanvitto, F. P. Laussy, D. Ballarini, E. d. Valle, M. D. Martin, A. Lemaître, J. Bloch, D. N. Krizhanovskii, M. S. Skolnick, C. Tejedor, and L. Viña, Collective fluid dynamics of a polariton condensate in a semiconductor microcavity, Nature **457**, 291 (2009).

[28] K. G. Lagoudakis, M. Wouters, M. Richard, A. Baas, I. Carusotto, R. André, L. S. Dang, and B. Deveaud-Plédran, Quantized vortices in an exciton–polariton condensate, Nature physics **4**, 706 (2008).

[29] D. Sanvitto, S. Pigeon, A. Amo, D. Ballarini, M. De Giorgi, I. Carusotto, R. Hivet, F. Pisanello, V. G. Sala, P. S. S. Guimaraes, R. Houdré, E. Giacobino, C. Ciuti, A. Bramati, and G. Gigli, All-optical control of the quantum flow of a polariton condensate, Nature Photonics **5**, 610 (2011).

[30] G. Nardin, G. Grosso, Y. Léger, B. Pietka, F. Morier-Genoud, and B. Deveaud-Plédran, Hydrodynamic nucleation of quantized vortex pairs in a polariton quantum fluid, Nature

Physics **7**, 635 (2011).

[31] R. Panico, G. Macorini, L. Dominici, A. Gianfrate, A. Fieramosca, M. De Giorgi, G. Gigli, D. Sanvitto, A. S. Lanotte, and D. Ballarini, Dynamics of a vortex lattice in an expanding polariton quantum fluid, Phys. Rev. Lett. **127**, 047401 (2021).

[32] T. Ozawa, H. M. Price, A. Amo, N. Goldman, M. Hafezi, L. Lu, M. C. Rechtsman, D. Schuster, J. Simon, O. Zilberberg, and I. Carusotto, Topological photonics, Rev. Mod. Phys. **91**, 015006 (2019).

[33] S. Alyatkin, J. D. Töpfer, A. Askitopoulos, H. Sigurdsson, and P. G. Lagoudakis, Optical control of couplings in polariton condensate lattices, Phys. Rev. Lett. **124**, 207402 (2020).

[34] M. Pieczarka, E. Estrecho, S. Ghosh, M. Wurdack, M. Steger, D. W. Snoke, K. West, L. N. Pfeiffer, T. C. H. Liew, A. G. Truscott, and E. A. Ostrovskaya, Topological phase transition in an all-optical exciton-polariton lattice, Optica **8**, 1084 (2021).

[35] D. Caputo *et al.*, Topological order and thermal equilibrium in polariton condensates, Nat. Mater. **17**, 145 (2018).

[36] L. Galantucci, A. W. Baggaley, N. G. Parker, and C. F. Barenghi, Crossover from interaction to driven regimes in quantum vortex reconnections, Proceedings of the National Academy of Sciences **116**, 12204 (2019).

[37] A. Zamora, G. Dagvadorj, P. Comaron, I. Carusotto, N. P. Proukakis, and M. H. Szymańska, Kibble-Zurek mechanism in driven dissipative systems crossing a nonequilibrium phase transition, Phys. Rev. Lett. **125**, 095301 (2020).

[38] N. G. Berloff, Turbulence in exciton-polariton condensates, arXiv:1010.5225v2 (2010).

[39] S. Koniakhin, O. Bleu, G. Malpuech, and D. Solnyshkov, 2d quantum turbulence in a polariton quantum fluid, Chaos, Solitons & Fractals **132**, 109574 (2020).

[40] A. Skaugen and L. Angheluta, Vortex clustering and universal scaling laws in two-dimensional quantum turbulence, Phys. Rev. E **93** (2016).

[41] A. D. Garcia-Orozco, L. Madeira, L. Galantucci, C. F. Barenghi, and V. S. Bagnato, Intrascales energy transfer during the evolution of turbulence in a trapped Bose-Einstein condensate, Europhys. Lett. **130**, 46001 (2020).

[42] M. Steger, G. Liu, B. Nelsen, C. Gautham, D. W. Snoke, R. Balili, L. Pfeiffer, and K. West, Long-range ballistic motion and coherent flow of long-lifetime polaritons, Phys. Rev. B **88**, 235314 (2013).

[43] S. Alyatkin, H. Sigurdsson, A. Askitopoulos, J. D. Töpfer, and P. G. Lagoudakis, Quantum fluids of light in all-optical scatterer lattices, Nature Communications **12**, 5571 (2021).

[44] E. Wertz, L. Ferrier, D. D. Solnyshkov, R. Johne, D. Sanvitto, A. Lemaître, I. Sagnes, R. Grousson, A. V. Kavokin, P. Senellart, G. Malpuech, and J. Bloch, Spontaneous formation and optical manipulation of extended polariton condensates, Nature Physics **6**, 860 (2010).

[45] S. Donati, L. Dominici, G. Dagvadorj, D. Ballarini, M. De Giorgi, A. Bramati, G. Gigli, Y. G. Rubo, M. H. Szymańska, and D. Sanvitto, Twist of generalized skyrmions and spin vortices in a polariton superfluid, Proceedings of the National Academy of Sciences **113**, 14926 (2016).

[46] R. N. Valani, A. J. Groszek, and T. P. Simula, Einstein–Bose condensation of onsager vortices, New Journal of Physics **20**, 053038 (2018).

[47] G. V. Kolmakov, P. V. E. McClintock, and S. V. Nazarenko, Wave turbulence in quantum fluids, Proceedings of the National Academy of Sciences **111**, 4727 (2014).

[48] T. Kanai and W. Guo, True mechanism of spontaneous order from turbulence in two-dimensional superfluid manifolds, Phys. Rev. Lett. **127**, 095301 (2021).

[49] A. S. Bradley, R. K. Kumar, S. Pal, and X. Yu, Spectral analysis for compressible quantum fluids, Phys. Rev. A **106**, 043322 (2022).

[50] A. N. Kolmogorov, The local structure of turbulence in incompressible viscous fluid for very large reynolds numbers, C. R. Acad. Sci. URSS **30**, 301 (1941).

[51] P. Comaron, I. Carusotto, M. H. Szymańska, and N. P. Proukakis, Non-equilibrium Berezinskii-Kosterlitz-Thouless transition in driven-dissipative condensates (a), EPL (Europhysics Letters) **133**, 17002 (2021).

[52] K. Lagoudakis *et al.*, Probing the dynamics of spontaneous quantum vortices in polariton superfluids, Phys. Rev. Lett. **106**, 115301 (2011).

[53] D. Caputo, N. Bobrovska, D. Ballarini, M. Matuszewski, M. De Giorgi, L. Dominici, K. West, L. N. Pfeiffer, G. Gigli, and D. Sanvitto, Josephson vortices induced by phase twisting a polariton superfluid, Nature Photonics **13**, 488 (2019).

[54] C. Michel, O. Boughdad, M. Albert, P.-E. Larré, and M. Bellec, Superfluid motion and drag-force cancellation in a fluid of light, Nature Communications **9**, 2108 (2018).

[55] G. Situ and J. W. Fleischer, Dynamics of the Berezinskii–Kosterlitz–Thouless transition in a photon fluid, Nature Photonics **14**, 517 (2020).

[56] C. Piekarski, W. Liu, J. Steinhauer, E. Giacobino, A. Bramati, and Q. Glorieux, Measurement

of the static structure factor in a paraxial fluid of light using Bragg-like spectroscopy, Phys. Rev. Lett. **127**, 023401 (2021).

[57] L. W. Clark, N. Schine, C. Baum, N. Jia, and J. Simon, Observation of Laughlin states made of light, Nature **582**, 41 (2020).

[58] I. Shelykh, G. Malpuech, K. V. Kavokin, A. V. Kavokin, and P. Bigenwald, Spin dynamics of interacting exciton polaritons in microcavities, Phys. Rev. B **70**, 115301 (2004).